Phase-field study of the second phase particle effect on texture evolution of polycrystalline material*

Lu Yan-Li(卢艳丽)†, Zhang Liu-Chao(张刘超), Zhou Ying-Ying(周影影), and Chen Zheng(陈 铮)

State Key Laboratory of Solidification Processing, Northwestern Polytechnical University, Xi'an 710072, *China*

(Received 17 October 2013; revised manuscript received 5 December 2013; published online 20 April 2014)

The second phase particle effect on texture evolution of polycrystalline material is studied through phase-field method. A unique field variable is introduced into the phase-field model to represent the second phase particles. Elastic interaction between particles and grains is also considered. Results indicate that in the presence of second phase particles the average particle diameter turns smaller than in the absence of these particles and retards texture formation by pinning effect. The second phase particles change the strain energy profile, which tremendously influences the pinning effect.

Keywords: texture evolution, second phase particles, elastic energy, phase-field method

PACS: 91.60.Ed, 81.40.Jj, 81.40.Lm **DOI:** 10.1088/1674-1056/23/6/069102

1. Introduction

Material microstructure, especially texture and grain size, have very important effects on the mechanical and physical behaviors of a material.[1–5] The influence of texture on mechanical property accounts for 20%–50% of the property value.[6] Ultrafine-grained material with grain size smaller than 1 μm exhibits superior mechanical properties, such as high strength, high toughness, good fatigue strength, and excellent superplasticity.[7,8] Therefore, the controlling of texture and grain size is important for material design.[9–12] Several researchers have shown great interest in the effects of the second phase particles on texture evolution and grain growth.[13–15] Li *et al*.[16] investigated the effects of the second phase particles on the deformation mechanisms and the resulting texture by studying the texture evolutions of three kinds of Al–Zn–Mg alloys. In addition, Malick[17] studied the influence of monodispersed mobile second phase particles on polycrystalline grain growth.

With the development of computer technology, the phase-field dynamic model has become a powerful computational approach to modeling and predicting mesoscale morphological and microstructure evolutions in materials.[18–21] In most studies[16,17] of the effect of the second phase particles, only the bulk free energy of particles is considered when, in fact, the elastic strain energy caused by a coherent misfit also plays a very important role in texture evolution and grain growth. In this paper, we introduce the second phase particles into the phase-field model developed by Chen and Bnottacharyya[22] to study their effect on polycrystalline material microstructure evolution. The focus is mainly on the effect of the second phase particles on texture evolution and the pinning effect of particles in an elastic constrained system.

2. Phase-field model

In the phase-field approach, a set of continuous nonconserved parameter fields $\eta_g(r,t)$ $(g = 1....Q)$ is used to represent the orientation of each grain. The second phase particle is denoted as $p(r)$: inside the second phase particle $p(r) = 1$ and outside the particle $p(r) = 0$. The function $\phi(r,t) = \sum_{g=1}^{Q} \eta_g^2(r,t)$ is used to distinguish the grain interior and the grain boundary.

The position-dependent stiffness tensor $C_{ijkl}(r)$ is a function of the stiffness tensor C_{pqrs} of the reference medium and the transformation matrix is expressed as[20]

$$C_{ijkl}(r) = \sum_g \phi_g a_{ip}^g a_{jq}^g a_{kr}^g a_{ls}^g C_{pqrs}, \tag{1}$$

where a_{ij}^g is the transformation matrix representing the rotation of the coordinate system defined on a given grain g with respect to the fixed reference, and is expressed in terms of the Euler angles θ, ψ, and ξ as follows:

$$a_{ij}^g = \begin{pmatrix} \cos\theta\cos\xi - \sin\theta\sin\xi\cos\psi & \sin\theta\cos\xi + \cos\theta\sin\xi\cos\psi & \sin\xi\sin\psi \\ -\cos\theta\sin\xi - \sin\theta\cos\xi\cos\psi & -\sin\theta\sin\xi + \cos\theta\cos\xi\cos\psi & \cos\xi\sin\psi \\ \sin\theta\sin\psi & -\cos\theta\sin\psi & \cos\psi \end{pmatrix}. \tag{2}$$

*Project supported by the National Natural Science Foundation of China (Grant Nos. 51174168, and 51274167) and "111" Project, China (Grant No. B08040).

†Corresponding author. E-mail: luyanli@nwpu.edu.cn

© 2014 Chinese Physical Society and IOP Publishing Ltd

In this model, only the Euler angle θ is considered in the simulation of a two-dimensional (2D) system, while ψ and ξ are set to be zero.

The spatially dependent elastic stiffness tensor $C_{ijkl}(r)$ can be written as a sum of a constant homogeneous part C^0_{ijkl} and a position-dependent inhomogeneous perturbation $C'_{ijkl}(r)$; that is,

$$C_{ijkl}(r) = C^0_{ijkl} + C'_{ijkl}, \tag{3}$$

$C_{ijkl}(r)$ can also be rewritten as

$$C_{ijkl}(r) = C^0_{ijkl} + \left(\sum_g \eta^0_g(r)\, a^g_{ip} a^g_{jq} a^g_{kr} a^g_{ls} C_{pqrs} - C^0_{ijkl} \right). \tag{4}$$

Letting $\varepsilon_{ij}(r)$ denote the total strain, under the assumption of linear elasticity, the local stress $\sigma_{ij}(r)$ can be given by[20]

$$\sigma_{ij}(r) = \left(C^0_{ijkl} + C'_{ijkl}(r) \right) \left(\varepsilon_{kl}(r) - \varepsilon^0_{kl}(r) \right). \tag{5}$$

Here, $\varepsilon^0_{kl}(r)$ is the stress-free eigenstrain field that can arise from phase transformation. Since phase transformation is not considered in this model, $\varepsilon^0_{kl}(r)$ is set to be zero.

The local elastic field can be obtained by solving the mechanical equilibrium equation

$$\frac{\partial \sigma_{ij}}{\partial r_j} = 0, \quad \text{i.e.,} \quad \nabla_j C_{ijkl}(r) \left(\varepsilon_{kl}(r) - \varepsilon^0_{kl}(r) \right) = 0. \tag{6}$$

The total strain $\varepsilon_{ij}(r)$ can be expressed as a sum of homogeneous and heterogeneous strains; that is,[23]

$$\varepsilon_{ij}(r) = \bar{\varepsilon}_{ij} + \delta\varepsilon_{ij}(r). \tag{7}$$

The homogeneous strain $\bar{\varepsilon}_{ij}$ is defined as

$$\int \delta\varepsilon_{ij}(r)\, \mathrm{d}^3 r = 0. \tag{8}$$

The heterogeneous strain field $\delta\varepsilon_{ij}(r)$ is defined by the displacement field as

$$\delta\varepsilon_{ij}(r) = \frac{1}{2} \left(\frac{\partial u_i(r)}{\partial r_j} + \frac{\partial u_j(r)}{\partial r_i} \right). \tag{9}$$

By substituting Eqs. (8) and (9) into Eq. (6), we obtain

$$\nabla_j C_{ijkl}(r) \left[\bar{\varepsilon}_{kl} + \frac{1}{2} \left(\frac{\partial u_k(r)}{\partial r_l} + \frac{\partial u_l(r)}{\partial r_k} \right) - \varepsilon^0_{kl}(r) \right] = 0. \tag{10}$$

By rearranging and simplifying Eq. (10), we obtain

$$\begin{aligned} & C^0_{ijkl} \frac{\partial^2 u_k(r)}{\partial r_j \partial r_l} \\ &= \nabla_j \left\{ \left(\sum_g \eta^2_g(r)\, a^g_{ip} a^g_{jq} a^g_{kr} a^g_{ls} C_{pqrs} \right) \left(\varepsilon^0_{kl} - \bar{\varepsilon}_{kl} \right) \right\} \\ & - \frac{\partial}{\partial r_j} \left[\left(\sum_g \eta^2_g(r)\, a^g_{ip} a^g_{jq} a^g_{kr} a^g_{ls} C_{pqrs} - C^0_{ijkl} \right) \frac{\partial u_k(r)}{\partial r_l} \right]. \end{aligned} \tag{11}$$

The temporal evolution of the non-conserved parameter field $\eta_g(r)$ $(g = 1, \ldots, Q)$ is described by the Cahn–Allen equation as follows:

$$\frac{\partial \eta_g(r,t)}{\partial t} = -L_g \left(u_{\mathrm{ch}} + u_{\mathrm{el}} \right), \tag{12}$$

where L_g is the relaxation coefficient, u_{ch} and u_{el} denote the derivations of the chemical and elastic parts of the free energy with respect to $\eta_g(r,t)$, respectively. u_{ch} is given by

$$u_{\mathrm{ch}} = \frac{\partial f(\eta_g(r,t))}{\partial \eta_g(r,t)} - 2Kg\nabla^2 \eta_g(r,t). \tag{13}$$

The homogeneous-free energy density $f(\eta_g(r,t))$ is formulated as a Landau polynomial of the phase-field variables $\eta_g(r,t)$ and $p(r)$ as follows:

$$\begin{aligned} & f(\eta_1, \eta_2, \ldots, \eta_Q) \\ &= \sum_{i=1}^{Q} \left(-\frac{\eta_i^2}{2} + \frac{\eta_i^4}{4} \right) + \sum_{i=1}^{Q} \sum_{j \neq i}^{Q} \eta_i^2 \eta_j^2 + \varepsilon \sum_{i=1}^{Q} \eta_i^2 p^2. \end{aligned} \tag{14}$$

Inside the second phase particle $p(r) = 1$, the homogeneous-free energy has a single minimum at $(\eta_1, \eta_2, \ldots, \eta_Q) = (0, 0, \ldots, 0)$.

u_{el} is obtained as

$$u_{\mathrm{el}} = \frac{\partial F_{\mathrm{el}}}{\partial \eta_g} = 2\eta_g \frac{\partial F_{\mathrm{el}}}{\partial \eta_g^2}. \tag{15}$$

When the difference in modulus and the difference in volume difference between the grain boundaries and the interior are ignored and the position-dependent eigenstrain tensor $\varepsilon^0_{ij}(r)$ is set to be zero, the elastic driving force u_{el} can be given by

$$\begin{aligned} u_{\mathrm{el}}(r) \;=\; & \eta_g(r) a^g_{ip} a^g_{jq} a^g_{kr} a^g_{ls} C_{pqrs} \\ & \times \left(\delta\varepsilon_{kl}(r) + \bar{\varepsilon}_{ij} \bar{\varepsilon}_{kl} + 2\delta\varepsilon_{ij}(r) \bar{\varepsilon}_{kl} \right). \end{aligned} \tag{16}$$

3. Results and discussion

In this paper, we present the simulation results for 2D microstructure evolutions of texture and grain growth in the presence of immobile second phase particles. The simulation domain size is set to be 512×512 grid points to ensure grain sufficiency at later stages. The grid size Δx is set to be 2.0, time step $\Delta t = 0.1$. In Eq. (14) ε is set to be 1.0, and K_g in Eq. (13) is set to be 1.0. The system in this simulation contains about 1500 grains with arbitrary crystalline orientations and equiaxed grain size serves as the initial microstructure.

Figure 1 shows the microstructure evolutions of systems with and without the second phase particles under uniaxial applied stress; the second phase particles are represented by dark circles. Figures 1(a1)–1(c1) show the microstructure evolutions of the system in the case without second phase particles (NP) at different times. The figures show that the grains gradually grow with time going by. Figures 1(a2)–1(c2) show the microstructure evolutions of a system in the case with second phase particles (YP) at corresponding times. Most of second particles are located on the grain boundaries. At later stages, the average particle diameter of the YP system turns much smaller than that of the NP system.

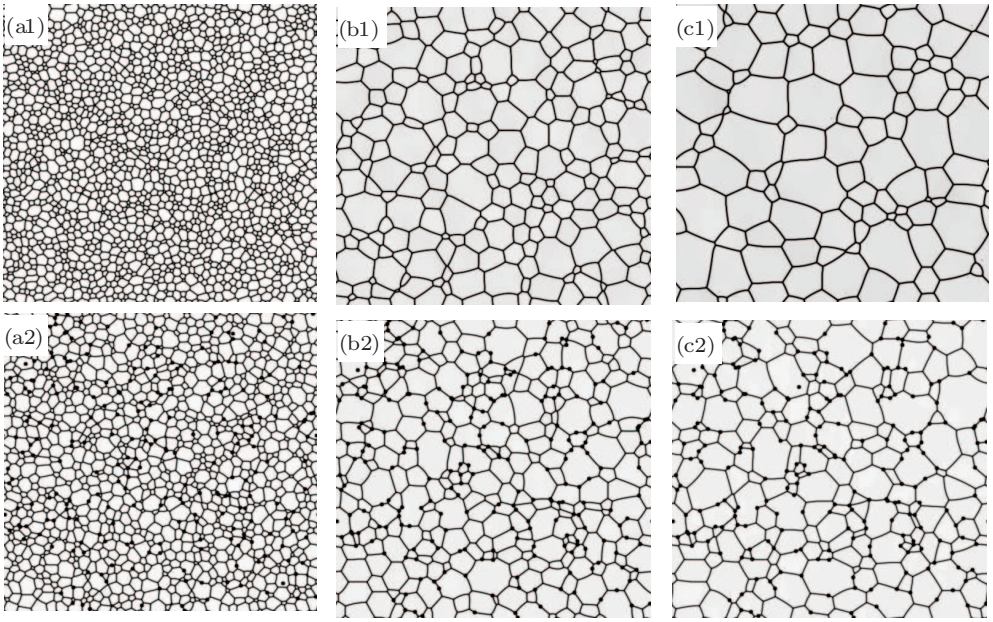


Fig. 1. Microstructure evolutions of NP and YP systems under uniaxial applied stress $\sigma_{xx} = 3.0$ GPa. (a1) NP system at $t = 10^3$, (b1) NP system at $t = 2.6 \times 10^3$, (c1) NP system at $t = 5 \times 10^4$. (a2) YP system at $t = 10^3$, (b2) YP system at $t = 2.6 \times 10^4$, (c2) YP system at $t = 5 \times 10^4$.

To investigate the texture evolutions of the two systems, we count the fractions of grain boundary orientation at different times, as shown in Fig. 2. The fractions of grain boundary orientation in the NP system at times 10^3, 2.6×10^4, and 5×10^4 are shown in Figs. 2(a1), 2(b1), and 2(c1), respectively. The fractions of grain boundary orientation in the YP system are shown in Figs. 2(a2), 2(b2), and 2(c2). Based on these figures, at the initial stage, all orientations in both systems have almost the same fraction. As time goes by, the fractions of some orientations in the NP system increase. At the final stage, some obviously preferred components can be found in the NP system. By contrast, no preferred orientation can be found in the YP system; that is, no strong texture exists in the YP system. Our simulation result is consistent with the experimental result observed by Li *et al.*[16]

To study the mechanism behind the effect of second phase particles on texture evolution, the grain boundary migration in a bi-crystal system with a second phase particle is simulated (Fig. 3). The elastic energy (defined as $f_{\text{els}} = C_{ijkl}(r)\varepsilon^{\text{el}}_{ij}(r)\varepsilon^{\text{el}}_{kl}(r)$), elastic potential (defined as $f_{\text{pot}} = \left(C_{ijkl}(r) - C_{pqrs}\right)\varepsilon^{\text{el}}_{ij}(r)\varepsilon^{\text{el}}_{kl}(r)$), and elastic driving force u_{el} are also calculated.

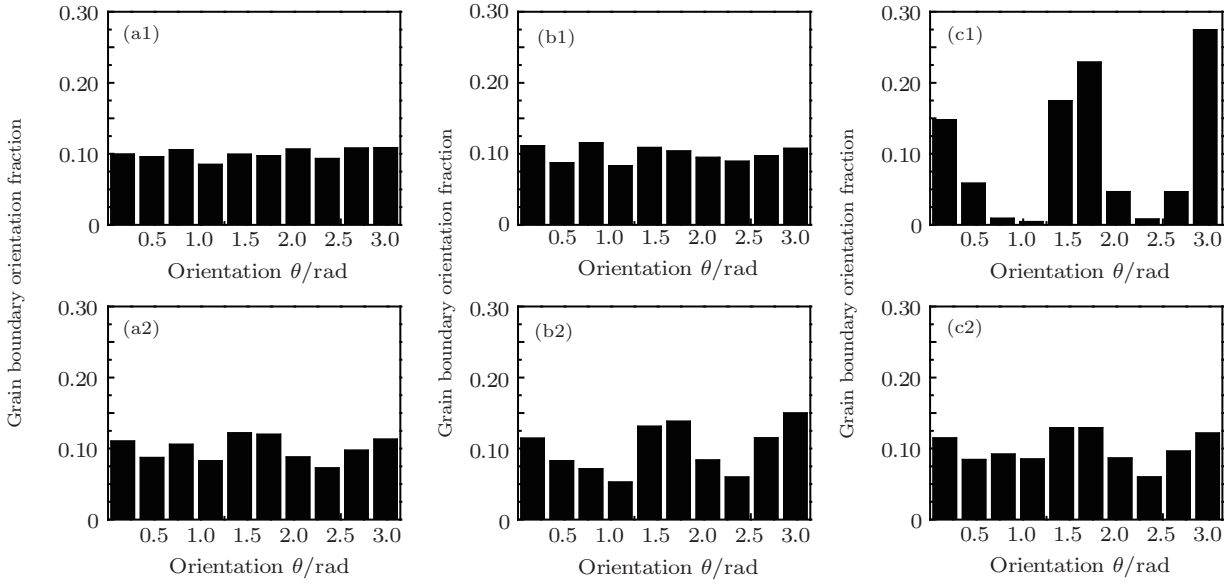


Fig. 2. Variations of grain boundary orientations of NP (panels (a1)–(c1)) and YP (panels (a2)–(c2)) systems with time. (a1) NP system at $t = 10^3$, (b1) NP system at $t = 2.6 \times 10^4$, (c1) NP system at $t = 5 \times 10^4$.

The grain boundary motion with time when the system is subjected to uniaxial stress $\sigma_{xx} = 3.0$ GPa, as shown in Fig. 3. The figure indicates that grain I (left, with $(\theta = 0)$ orientation) grows at the expense of grain II (right, with $(\theta = \pi/4)$ orientation), as proven by Chen.[18] More importantly, the grain boundary changes from a straight line to a curve, and the grain boundary near the second phase particle tends to grow toward the second particle, proving that the former has a pinning effect on the grain boundary.

The profiles of elastic energy and elastic potential are shown in Fig. 4. Grain I has a higher elastic energy and lower elastic potential, which is consistent with the simulation result of Chen.[18] More importantly, the elastic energy and elastic potential of the grain boundary near the second phase particle are much higher than elsewhere.

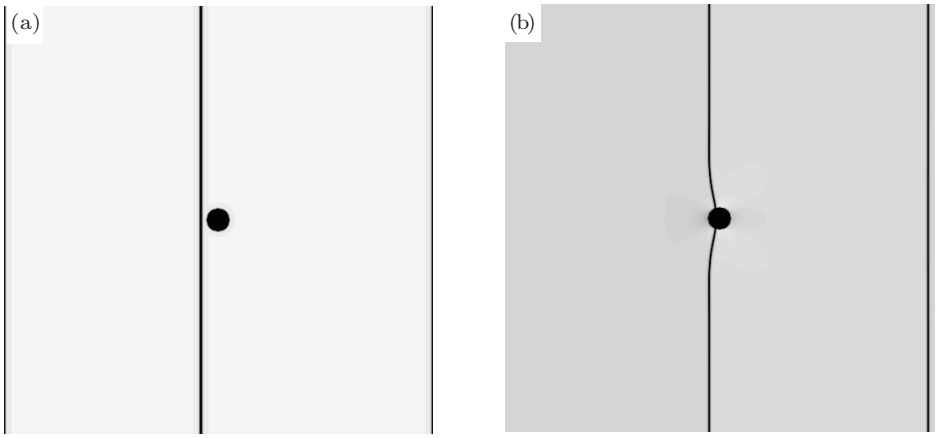


Fig. 3. Grain boundary motion of a bi-crystal system subjected to uniaxial applied stress $\sigma_{xx} = 3.0$ GPa at different times: (a) $t = 10^3$ and (b) $t = 3.6 \times 10^4$.

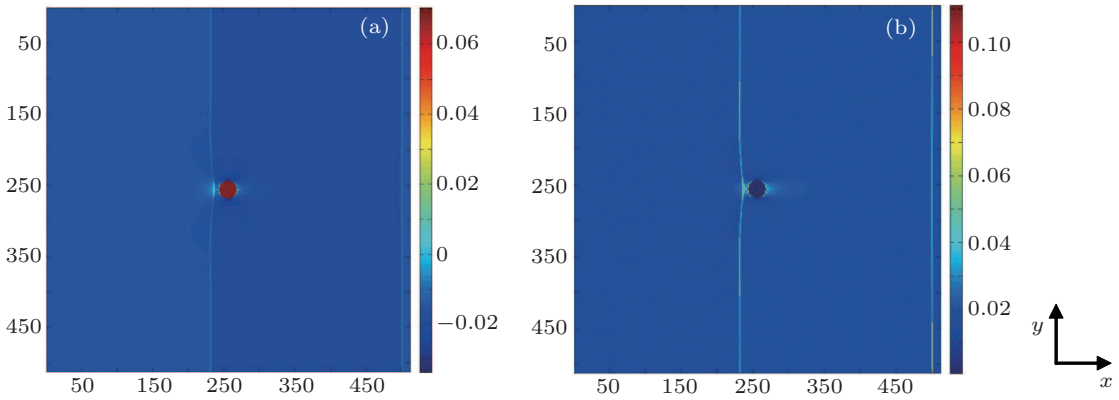


Fig. 4. (color online) (a) Elastic energy density profile of each grain; (b) elastic potential profile of each grain.

The elastic energy and elastic potential across the grain boundary at $y = 140$ and $y = 256$ are plotted in Figs. 5(a) and 5(b) to study the pinning effect of second phase particles on grain boundary. Figure 5(a) shows that the second phase particle results in a larger elastic energy of grain II than that of grain I, thus promoting the migration of grain boundary. The existence of second phase particles increases the difference in elastic potential between both sides of the grain boundary, as shown in Fig. 5(b). The elastic potential is a key parameter in determining the motion of grain boundary, so the occurrence of second phase particles results in a larger grain boundary motion velocity near the particle than elsewhere.

The existence of second phase particles influences the elastic energy and elastic potential of the system, resulting in the pinning effect on the grain boundary. These factors lead to more difficult growth of a grain with the preferred orientation and weakening texture in polycrystalline materials. Li *et al.*[16] obtained the same conclusion, and further proved that the deformation zone around the second phase particles has a higher than average deformation energy. High energy promotes the nucleation of recrystallization, and this process is called particle-stimulated nucleation. During the particle-stimulated nucleation, recrystallization nuclei develop with the characteristic orientation, thus affecting grain size and recrys-

tallization texture, and leading to grain refinement and texture randomization.

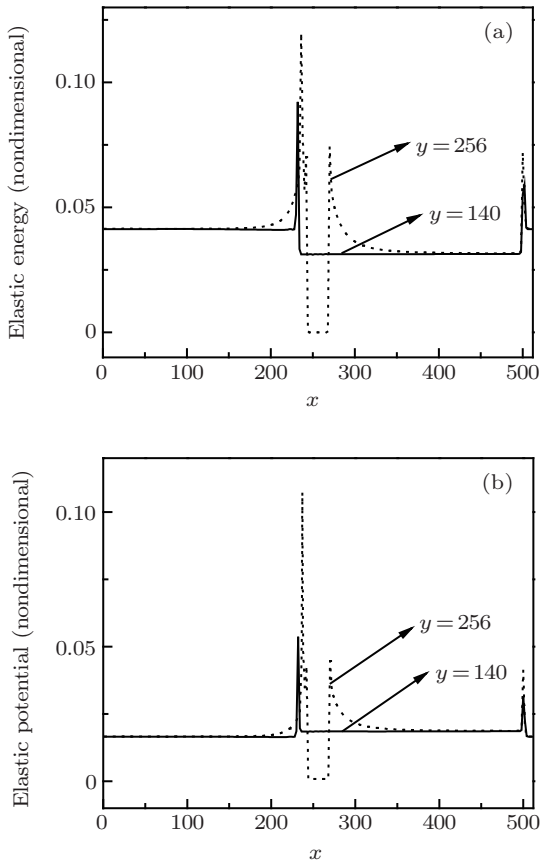


Fig. 5. (color online) (a) Elastic energy density profile at $y = 140$ and $y = 256$; (b) elastic potential profile at $y = 140$ and $y = 256$.

4. Conclusions

Second phase particles are introduced into the phase-field model to study the effect of the second phase particles on texture evolution under applied stress. Our results indicate that the existence of the second phase particles results in smaller average particle diameter than the nonexistence of these particles. Moreover, the formation of texture of polycrystalline material is retarded by the pinning effect. Further study shows that the elastic interaction between the grain boundary and the second phase particles plays a very important role in the pinning effect.

Acknowledgment

The authors sincerely thank professor Chen Long-Qing in the Department of Materials Science and Engineering, Penn State University of USA for his valuable discussion.

References

[1] Mallick A, Vedantam S and Lu L 2009 *Mater. Sci. Eng. A* **515** 14
[2] Dao M, Lu L, Asaro R J, De Hosson J T M and Ma E 2007 *Acta Mater.* **55** 4041
[3] Suwas S, Beausir B, Tóth L S, Fundenberger J J and Gottstein G 2011 *Acta Mater.* **59** 1121
[4] Song K and Aindow M 2008 *Mater. Sci. Eng. A* **479** 365
[5] Wang X P, Wang Z, Wang L J and Mei C Y 2011 *Chin. Phys. B* **20** 105203
[6] Engler O and Randle V 2010 *Introduction to Texture Analysis: Macrotexture, Microtexture, and Orientation Mapping*, 2nd edn. (New York: CRC Press) pp. 3–5
[7] Qi M L, Zhong S, He H L, Fan D and Zhao L 2013 *Chin. Phys. B.* **22** 046203
[8] Callister William D Jr 2007 *Materials Science and Engineering: an Introduction*, 7th edn. (New York: John Wiley & Sons) pp. 123–172
[9] Sidor J J, Petrov R H and Kestens L A I 2011 *Acta Mater.* **59** 5735
[10] Kim C S, Hu Y, Rohrer G S and Randle V 2005 *Scr. Mater.* **52** 633
[11] Gruber J, Miller H M, Miller T D, Rohrer G S and Rollett A D 2009 *Acta Mater.* **57** 6102
[12] Chen D M, Liu Y L, Li Y X, Yang K and Zhang H W 2012 *Chin. Phys. B* **21** 067502
[13] Schäfer C, Song J and Gottstein G 2009 *Acta Mater.* **57** 1026
[14] Hadorn J P, Hantzsche K, Yi S, Bohlen J, Letzig D and Agnew S R 2012 *Metall. Mater. Trans. A* **43** 1363
[15] Pirgazi H and Akbarzadeh A 2009 *Mater. Sci. Technol.* **25** 625
[16] Li X, Jiao F, Samman T A and Chowdhury S G 2012 *Scr. Mater.* **66** 159
[17] Mallick A 2013 *Comput. Mater. Sci.* **67** 27
[18] Chen L Q 2002 *Ann. Rev. Mater. Res.* **32** 113
[19] Wang Z J, Wang J C and Yang G C 2010 *Chin. Phys. B* **19** 017305
[20] Li J J, Wang J C and Yang G C 2008 *Chin. Phys. B* **17** 3516
[21] Zaeem M A and Mesarovic S D 2011 *Comput. Mater. Sci.* **50** 1030
[22] Bhattacharyya S, Heo T W, Chang K and Chen L Q 2011 *Modell. Simul. Mater. Sci. Eng.* **19** 035002
[23] Lu Y L, Zhang L C, Zhou Y Y, Chen Z and Zhang J G 2013 *J. Mater. Sci. Technol.* **29** 999